



A Wavelet-Based Metric for Visual Texture Discrimination with Applications in Evolutionary Ecology

RICHARD A. KILTIE

Department of Zoology, University of Florida, Gainesville, Florida

AND

JIAN FAN AND ANDREW F. LAINE

Department of Computer and Information Sciences, University of Florida, Gainesville, Florida

Received 24 January 1994; revised 8 June 1994

ABSTRACT

Much work on natural and sexual selection is concerned with the conspicuousness of visual patterns (textures) on animal and plant surfaces. Previous attempts by evolutionary biologists to quantify apparency of such textures have involved subjective estimates of conspicuousness or statistical analyses based on transect samples. We present a method based on wavelet analysis that avoids subjectivity and that uses more of the information in image textures than transects do. Like the human visual system for texture discrimination, and probably like that of other vertebrates, this method is based on localized analysis of orientation and frequency components of the patterns composing visual textures. As examples of the metric's utility, we present analyses of crypsis for tigers, zebras, and peppered moth morphs.

INTRODUCTION

Visual textures are spatially extended patterns based on the repetition of a unit cell or "texton" [28, 37]. Over the past 30 years, research concerning discrimination of visual textures has greatly expanded in the fields of psychophysics and computer vision. Psychobiologists like Julesz [36], Ramachandran [58–61], DeValois and DeValois [18], Arbib and Hanson [1], and Nakayama et al. [56] have suggested that the capacity for rapid ("preattentive") visual texture discrimination probably evolved under the influence of selective forces, especially by the need to "break" the camouflage of potential predators or prey. However, evolutionary and ecological biologists have made little direct use of advances in this area. This gap is notable because, at least since the time of Darwin [16], questions concerning concealment (camouflage) and apparency (advertisement) have been important to the development of

ideas on natural selection and sexual selection, respectively [20, 22, 24]. Hypotheses concerning visual effects of surface patterns continue to motivate much research both on animals and plants.

Most psychophysical studies of texture discrimination have concerned humans and other primates, but work with cats [77], falcons [26], and pigeons [3, 4, 63] suggests that basic principles of visual system design that relate to texture discrimination are shared among vertebrates. In some respects, these principles may even be shared with invertebrates [13, 68]. The neuroanatomical basis for texture discrimination seems to lie in cell groups in the visual pathway that are responsive to specific orientation and frequency components of images [18, 33, 34, 74]. Computational techniques based on “wavelets,” which perform localized frequency and orientation analysis, therefore show great promise in modeling systems for visual texture discrimination [35, 46, 49, 51, 74, 76].

Our purpose in this paper is to present a texture-discrimination metric that incorporates recent advances in computational vision and psychobiology and that will be useful to evolutionary and ecological biologists interested in quantitatively assessing the conspicuousness of visual textures of plants and animals to vertebrate viewers in natural settings. Work having this aim has been needed because most prior applications of texture discrimination in computer vision research and psychobiology have involved simple binary patterns or relatively uniform grayscale textures. In natural scenes (without anthropogenic content), there is nearly always some irregularity or gradual variation within surface textures, and intensity variation is continuous. Another limitation of much previous work has been its emphasis on qualitative, pairwise discriminability between textures (so that texture pairs are judged simply as discriminable or not). In reality, of course, there may be degrees of discriminability among natural textures [19, 45, 48, 52]. It would be desirable to have a well-validated metric that can indicate relative discriminability of any textures, even those that have not been directly assessed psychophysically. Such a metric would accommodate statistical tests on replicate samples (e.g., analysis of variance) that ecological and evolutionary biologists typically use.

Although there has been considerable interest in psychophysical influences on the evolution of coloration and color patterns among animals (e.g., [8, 15, 22, 29, 31, 40, 57, 71]), visual textures as such have been little addressed in this context [43, 66]. Pattern has been analyzed primarily by transect methods [21, 23, 39, 41, 42, 44, 70] or by methods requiring subjective identification of individual pattern elements, followed by objective measurement of each element’s color (e.g., [25]). Computational image-analysis techniques will be essential in order to

deal with all of the information in visual textures of natural scenes and from animals with complicated or subtle coat patterns.

METHODS

Laine and Fan [46] used a wavelet-packet analysis to produce a highly effective framework for texture classification after training the system on a set of known textures. Our objective was to extend their approach so that distances among any pair of textures could be computed without prior training.

INTRODUCTION TO WAVELET ANALYSIS

Fourier analysis has long been used for signal analysis. For a stationary sinusoid signal, its Fourier transform is a Dirac impulse [5] which precisely indicates the frequency of the signal. For nonstationary signals, it is well known that a Fourier transform can reflect only global frequency content and cannot capture frequency evolution over time. In order to analyze a signal's behavior around a specific time, a window is usually applied to the signal and an analysis is conducted on the windowed segment.

The wavelet transform may be viewed as a windowed transformation technique [17, 49, 64]. A continuous wavelet transform can be written as

$$CW_s(\tau, a) = \int_{-\infty}^{\infty} s(x) \psi_a(x - \tau) dx, \quad (1)$$

where $\psi_a(x) = 1/\sqrt{|a|} \psi(x/a)$ and $\psi(t)$ is called the basic wavelet, satisfying the condition

$$C_\psi = \int_0^{\infty} \frac{|\psi(\omega)|^2}{\omega} d\omega < +\infty.$$

Parameter τ is a translation factor, and a is a dilation factor. When a increases, the function $\psi_a(x - \tau)$ expands and takes longtime behavior into account. In the opposite case, when a decreases, the function $\psi_a(x - \tau)$ contracts and focuses only on the short time behavior. Such a transformation is invertible such that the original signal may be recovered from its wavelet transform

$$s(x) = \frac{1}{C_\psi} \int_{\tau=-\infty}^{\tau=\infty} \int_{a=0}^{a=\infty} CW_s(\tau, a) \psi_a(x - \tau) \frac{d\tau da}{a^2}. \quad (2)$$

The continuous wavelet transform shown above is a highly redundant representation. A series representation instead of the integral can be obtained by sampling the parameters $a = 2^j$ and $\tau = n2^j$. Such a series is called a discrete wavelet transform and can be written as

$$s(x) = \sum_{j \in \mathbb{Z}} \sum_{n \in \mathbb{Z}} \mu_n^j \psi_{2^j}(x - n2^j). \quad (3)$$

For the construction of wavelets, a scaling function $\phi(x)$ is introduced, which should satisfy the dilation equation

$$\phi(x) = \sqrt{2} \sum_k h_k \phi(2x - k).$$

A wavelet may then be constructed from the scaling function $\phi(x)$

$$\psi(x) = \sqrt{2} \sum_k g_k \phi(2x - k),$$

where h_k and g_k are low-pass and high-pass discrete filters, respectively. (A low-pass filter eliminates information above a set frequency and a high-pass filter does the opposite.)

Daubechies [17], Meyer [53], and Stromberg [69] independently found that there exists some wavelet $\psi(t) \in L^2(\mathbf{R})$ such that $\{\psi_{2^j}(t - n2^j) |_{(n,j) \in \mathbb{Z}^2}\}$ forms an orthonormal basis of $L^2(\mathbf{R})$. Such wavelets are called *orthogonal wavelets*. The discrete filters associated with orthogonal wavelets are *quadrature mirror filters* (QMF) [17, 49, 73] satisfying the condition

$$\begin{aligned} |H(\omega)|^2 + |H(\omega + \pi)|^2 &= 1, \\ H(\omega)H^*(\omega + \pi) - H^*(\omega)H(\omega + \pi) &= 0, \end{aligned}$$

and

$$G(\omega) = -e^{-j\omega}H^*(\omega + \pi),$$

where $H(\omega) = \frac{1}{\sqrt{2}} \sum_k h_k e^{-jk\omega}$ and $G(\omega) = \frac{1}{\sqrt{2}} \sum_k g_k e^{-jk\omega}$.

Using orthogonal wavelets, the coefficients μ_n^j of a discrete wavelet transform may be explicitly written as

$$\mu_n^j = \langle s(u), \psi_{2^j}(u - n2^j) \rangle,$$

where $\langle s(u), f(u) \rangle = \int_{-\infty}^{\infty} s(u)f(u) du$ represents the inner product of the two functions.

Wavelet packets [10–12] are a set of orthogonal basis functions $\{W^n(x) | n \in Z^+\}$ that refine the basic wavelet recursively as follows

$$W_{2^{p+1}}^{2n}(x - l2^{p+1}) = \sum_m h_{m-2l} W_{2^p}^n(x - m2^p) \quad (4)$$

$$W_{2^{p+1}}^{2n+1}(x - l2^{p+1}) = \sum_m g_{m-2l} W_{2^p}^n(x - m2^p) \quad (5)$$

with $W^0(x) = \phi(x)$, $W^1(x) = \psi(x)$, and

$$\begin{aligned} W_{2^p}^n(x - k2^p) &= \sum_l h_{k-2l} W_{2^{p+1}}^{2n}(x - l2^{p+1}) \\ &\quad + \sum_l g_{k-2l} W_{2^{p+1}}^{2n+1}(x - l2^{p+1}), \end{aligned} \quad (6)$$

where $W_a^n(x) = \frac{1}{\sqrt{|a|}} W^n(x/a)$.

A major advantage of this analysis is that wavelet packets are well localized in both time and frequency and thus provide an attractive alternative to pure frequency (Fourier) analysis.

NORMALIZED DISTANCE MEASURE FOR DISCRETE SIGNALS

In order to implement wavelet packet transforms for discrete signals, we first define

$$\mu_k^{p,n} = \langle s(u), W_{2^p}^n(x - k2^p) \rangle.$$

By using (4)–(6) we can write the decomposition equations as

$$\begin{aligned} \mu_l^{p+1,2n} &= \sum_m h_{m-2l} \mu_m^{p,n}, \\ \mu_l^{p+1,2n+1} &= \sum_m g_{m-2l} \mu_m^{p,n}, \end{aligned}$$

and the reconstruction equation

$$\mu_k^{p,n} = \sum_l h_{k-2l} \mu_l^{p+1,2n} + \sum_l g_{k-2l} \mu_l^{p+1,2n+1}.$$

The extension for two-dimensional signals is straightforward by using a special class of separable two-dimensional wavelet packets $\{W_{2^p}^n(x -$

$l2^p)W_{2^p}^m(y - k2^p)$. The decomposition formulae now become

$$\begin{aligned} \mu_{b,d}^{p+1,2n,2m} &= \sum_l \sum_k h_{l-2b} h_{k-2d} \mu_{l,k}^{p,n,m}, \\ \mu_{b,d}^{p+1,2n,2m+1} &= \sum_l \sum_k h_{l-2b} g_{k-2d} \mu_{l,k}^{p,n,m}, \\ \mu_{b,d}^{p+1,2n+1,2m} &= \sum_l \sum_k g_{l-2b} h_{k-2d} \mu_{l,k}^{p,n,m}, \\ \mu_{b,d}^{p+1,2n+1,2m+1} &= \sum_l \sum_k g_{l-2b} g_{k-2d} \mu_{l,k}^{p,n,m}, \end{aligned}$$

and the reconstruction formula becomes

$$\begin{aligned} \mu_{l,k}^{p,n,m} &= \sum_b \sum_d h_{l-2b} h_{k-2d} \mu_{b,d}^{p+1,2n,2m} + \sum_b \sum_d h_{l-2b} g_{k-2d} \mu_{b,d}^{p+1,2n,2m+1} \\ &+ \sum_b \sum_d g_{l-2b} h_{k-2d} \mu_{b,d}^{p+1,2n+1,2m} \\ &+ \sum_b \sum_d g_{l-2b} g_{k-2d} \mu_{b,d}^{p+1,2n+1,2m+1}. \end{aligned}$$

Figure 1 illustrates a tree structure for the decomposition-reconstruction processes. The topmost node represents the original image (a

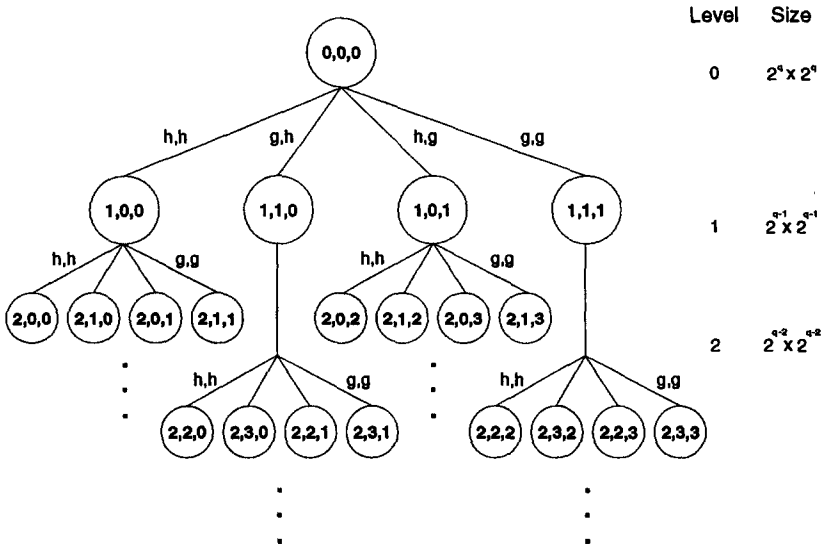


FIG. 1. Tree structure of a two-dimensional wavelet packet analysis. Each node represents a two-dimensional matrix $\mu^{p,n,m}$ of pixels (an image). Indices p, n, m of $\mu^{p,n,m}$ are shown for each node ($0,0,0$ is the original image). Links between nodes represent one-dimensional filters applied to columns and rows of each “parent” image to produce four “children,” as described in the text. Top-down computation is a decomposition process, and bottom-up is a reconstruction process.

matrix of pixels of size $2^q \times 2^q$). The links between nodes are one-dimensional filters that pass only low-frequency information (filter h , a low-pass filter) or high-frequency information (filter g , a high-pass filter) from rows and columns of a parent node to the four children nodes (images) that can be produced from it. The sizes of children are quartered by a subsequent decimation (downsampling) operation (one sample out of two adjacent samples is kept) on columns and rows. Orientation selectivity is determined by the particular combination of filters applied at each link: Horizontal components result from applying a low-pass filter h to rows and a high-pass g filter to columns; vertical components result from applying g to rows and h to columns; diagonal components result from applying g to both rows and columns. Orientation- and frequency-specific information can thus be isolated (image decomposition) at each level by the appropriate combination of filters. Reconstruction is the opposite process; every four nodes will generate a parent node by applying filtering and an *upsampling* operator (insert a zero between two adjacent samples).

We then define an energy measure

$$E^{p,n,m} = \sum_l \sum_k (\mu_{l,k}^{p,n,m})^2$$

for each component. We can show that

$$E^{p,n,m} = E^{p+1,2n,2m} + E^{p+1,2n+1,2m} + E^{p+1,2n,2m+1} + E^{p+1,2n+1,2m+1}.$$

Thus energy conservation exists between a parent and children.

We used energy values to construct the feature vector:

$$\{E^{n,m,p} \mid [0 \leq n \leq (2^p - 1), 0 \leq m \leq (2^p - 1)] \wedge (n+m > 0)\}. \quad (7)$$

Notice that $E^{0,0,p}$ is excluded from the feature vector due to the fact that its value is typically hundreds of times greater in magnitude. Therefore, for level p the vector length was $4^p - 1$. Such a feature vector characterizes the energy (variance) distribution for different frequencies (scales).

To compare two texture images, a simple discrimination measure was constructed as a normalized Euclidean distance defined by

$$D = \frac{(\sum_n |x_n - y_n|^2)^{1/2}}{(\sum_n |x_n|^2)^{1/2} + (\sum_n |y_n|^2)^{1/2}}, \quad (8)$$

where $X = \{x_n | 1 \leq n \leq N\}$ and $Y = \{y_n | 1 \leq n \leq N\}$ are two feature vectors and $0 \leq D \leq 1$ [72]. D thus reflects the degree of similarity of energy distribution patterns between images.

Our implementation of these equations requires square images with dimensions that are a power of 2. Depending on the size and resolution of the original image, and depending on the shapes of texture regions in the image, it may be necessary to analyze replicate square subsamples of a texture area (e.g., 64×64 pixels from a larger image) so that mean or median D values can be compared. Because subsamples within texture areas may differ among themselves, ratios of among-group D to within-group D could be used as a similarity measure that takes into account within-background variability. Effects of resolution and orientation can be addressed by reconstructing the images from specific frequency or orientation components. Some examples are presented later in this paper; see also Kiltie and Laine [43].

When the emphasis is on camouflage, as in our examples below, it is convenient to define a crypsis metric $C = 1 - D$, where D has been measured between the texture of some foreground object or organism and that of its background.

Executable binary programs (Sun Sparc architecture, Solaris 4.1.3) for obtaining feature vectors from raw images and for determining D can be obtained by contacting the first author (kiltie@nervm.nerdc.ufl.edu). For readers desiring more general information on wavelet analysis and programs, we suggest using the "Veronica" search facility via "Gopher" or "World Wide Web" on the internet.

TESTS WITH TEXTURES OF KNOWN DISCRIMINABILITY

The success of Laine and Fan's [46] results for classifying textures provided some confidence in our extension to a distance metric. However, the textures [7] that they used have not been subjected to psychophysical tests of discriminability, and hence could not be used to validate the D metric. We used three sets of published images to compare our metric with psychophysical assessments of texture distance.

Mayhew and Frisby [52] determined average times for human subjects to discriminate among six gray-scale images varying in orientation or frequency. These textures were presented in panels of four images, of which three were the same, and the time taken by the subject to identify the panel differing from the other three was measured. As expected, our D metric was highly, negatively correlated (Spearman $r = -0.90$) with these response times.

Beck et al. [2] published a series of pairs of gray-scale textures that were classified either as discriminable or not. We determined D for

each of these pairs, and then performed an analysis of variance with D as the criterion variable and discriminability (yes or no) as the predictor. The result was significant ($t = 2.85$, $df = 9$, $P = 0.02$).

Malik and Perona [48] summarized discriminability of 10 pairs of 1-bit/pixel (binary black and white) microtextures from Krose [45] and from Gurnsey and Browse [30], plus their own metric designed for 1-bit/pixel microtextures. Our metric produced an average Spearman correlation of 0.55 with these three measures (0.21 for Krose, 0.80 for Gurnsey and Browse, 0.64 for Malik and Perona's measure). The lower correlation in these cases than for the previous two may reflect some peculiarity of 1-bit microtextures or digitizing noise.

More grayscale textures calibrated psychophysically for discriminability with a variety of species are desirable in order to test the metric further.

EXAMPLE APPLICATIONS

The following examples are intended only to illustrate potential uses of our metric. Of course, thorough investigation of these examples would require replicate images and tests of significance.

CRYPsis OF PEPPERED MOTH MORPHS (BISTON BETULARIA)

Virtually every introductory textbook of biology describes "industrial melanism" in the British peppered moth *Biston betularia* as an example of natural selection operating when the environment changes. Peppered morphs (*B. b. f. typica*) have become less common and melanistic morphs (*B. b. f. carbonaria*) more common where industrial air pollution has caused disappearance of lichens from tree bark and darkening of the bark itself [38]. The change in morph frequencies has been attributed to selection by visual predators (birds) who search for the moths as they rest against tree trunks during the day and who capture *typica* more frequently and *carbonaria* less frequently in polluted areas. Whether selection by visual predators can explain observed changes in *B. betularia* morph frequencies has recently been questioned because the moths may not rest exposed on the tree bark as commonly as had been thought. However, it is still generally conceded that visual selection at least plays a part [6, 14, 32, 50].

Of course, it is obvious when glancing at the photographs in Figures 2 and 3 that the *typica* morphs match lichens better than *carbonaria* morphs, and that *carbonaria* morphs match polluted tree bark better than *typica*. However, after digitizing Figure 2 (500×455 pixels) and Figure 3 (320×510 pixels), the mean and median intensities for both morphs differ appreciably from the means and medians of both back-

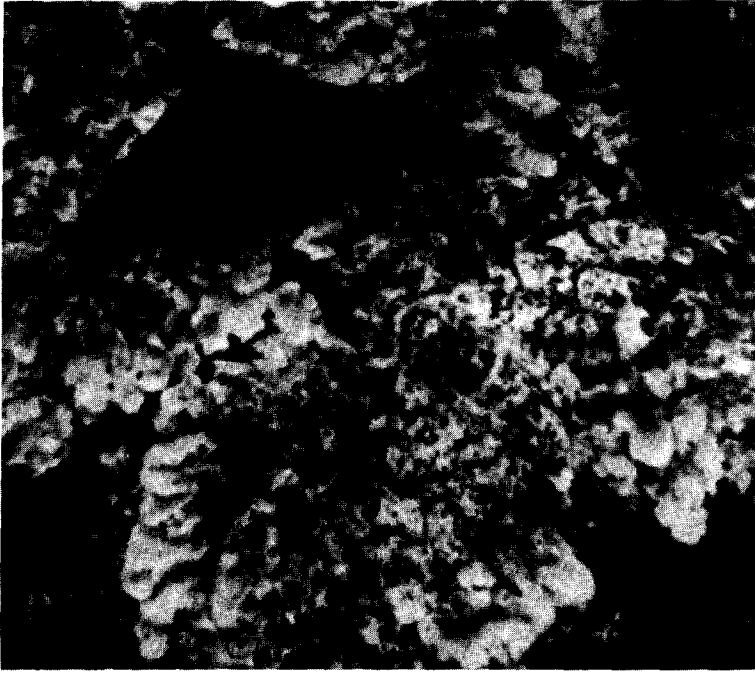


FIG. 2. *Biston betularia* f. *typica* (pale morph) and *B. b. f. carbonaria* (melanic morph) photographed against a lichen-covered tree trunk. This figure was reprinted from B. Kettlewell's *The Evolution of Melanism*, Oxford University Press, 1973 by permission of Oxford University Press.

grounds as in Table 1. Both morphs would be readily detectable against both backgrounds if spatial patterns of intensity variation (i.e., surface texture) of the morphs did not also match spatial intensity variation of the backgrounds against which they are cryptic. Because our metric incorporates the spatial element of intensity variation, it more accurately indicates the perceived differences in crypsis of the two morphs against the two backgrounds than do the first-order statistics of intensity variation.

From Figures 2 and 3 we took three 64×64 subsamples of each of the moths and six 64×64 subsamples of the backgrounds and then determined D and C values for the morphs versus their backgrounds and among the background samples themselves.

When information from all frequency levels in the images is included, average C for the *typica* subsamples from Figure 2 is high and is virtually the same as the average C between the subsamples of lichen background itself as in Figure 4. For subsamples of *carbonaria* from



FIG. 3. *Biston betularia* f. *typica* and *B. b.* f. *carbonaria* photographed against a pollution-darkened tree trunk. This figure was reprinted from B. Kettlewell's *The Evolution of Melanism*, Oxford University Press, 1973 with permission.

Figure 2, average C is much lower than for *typica* when all frequency information is included.

The wavelet-based reconstruction technique described earlier allows frequency-specific components of the images to be removed sequentially and cumulatively from high to low levels so that progressively lower-resolution reconstructions result. This permits consideration of changes in crypticity over a "gradient" from high-acuity viewers (diurnal

TABLE 1

Intensity Statistics for *Biston betularia* Morphs and Backgrounds in Figures 2 and 3

Area	Figure 2* (500×455 pixels)				Figure 3* (320×510) pixels			
	Mean	Median	SD	N pixels	Mean	Median	SD	N pixels
<i>typica</i>	174	184	50.7	25731	206	225	40.7	12196
<i>carbonaria</i>	89	85	19.2	19450	139	130	35.4	9911
Background	144	141	54.4	182319	120	112	32.1	141093

*Absolute values are comparable within photos, but not between them. Intensity scale is 0 (darkest) to 255 (lightest).

species with cone retinal cells or those with large eyes) to low-acuity viewers (nocturnal species with rod retinal cells or those with small eyes). For *typica* morphs, C remains high as resolution decreases (Figure 4). For *carbonaria* morphs on the other hand, C increases as resolution declines, i.e., their crypsis improves (Figure 4).

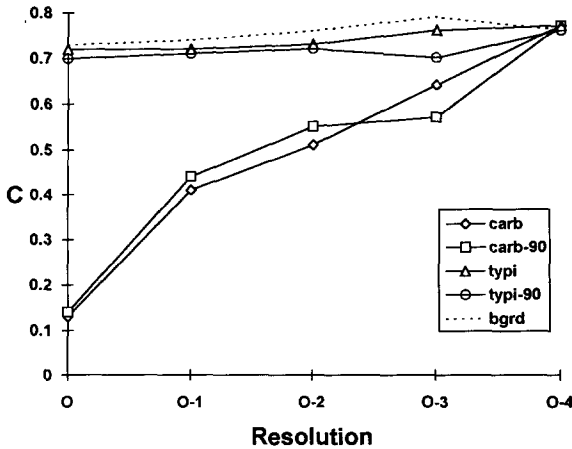


FIG. 4. Average crypsis index $C = 1 - D$ for three subsamples of each of the morphs of *Biston betularia* in Figure 2 versus six subsamples of the background. $C = 1$ is a perfect match "Carb" = *B. b. f. carbonaria*; "typi" = *B. b. f. typica*; "carb-90" = *carbonaria* after 90° rotation; "typi-90" = *B. b. f. typica* after 90° rotation; "bgrd" = average for comparisons among background subsamples themselves. "O" is the original resolution, and "O-x" refers to images that have had x upper frequency levels removed by wavelet-based reconstruction (e.g., see [43]).

Similar analyses were performed for the morphs against the darker tree bark in Figure 3. With all frequency levels included, average C for *carbonaria* against the dark background is about the same as average C between the subsamples of background themselves as in Figure 5. Average C for the *typica* subsamples is less than that for *carbonaria* with all frequencies included. Average C values for both morphs converge on the average C among background subsamples themselves as high-frequency information is stripped away, and the difference between *typica* and *carbonaria* in crypsis is negligible after two frequency levels have been excluded.

These results reinforce the idea that the relevant predators must be diurnal insectivores that inspect surfaces closely if visual selection is to account for changes in morph frequencies. Asymmetry between the morphs in the extent to which they match these kinds of backgrounds may contribute to some of the remaining uncertainty about the ability of visual predators to explain morph frequencies.

It has been of interest whether orientation of the moths' resting position is critical to their crypticity [38]. Our metric provides a way to address this question. We rotated by 90° each of the 64×64 pixel subsamples of the moths in Figures 2 and 3 while leaving the background subsamples unaltered and then recalculated the C values. Little or no change in C was produced against either background (Figures 4 and 5); thus, orientation appears to have little effect on camouflage for these moths.

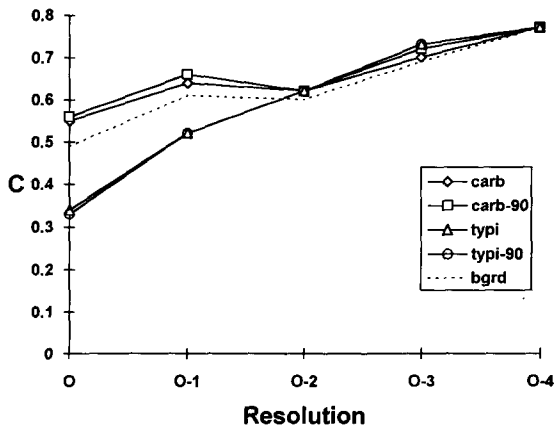


FIG. 5. Average crypsis index $C = 1 - D$ for three subsamples of each of the morphs of *Biston betularia* in Figure 3 versus six subsamples of the background. Abbreviations as in Figure 4.

ZEBRA AND TIGER STRIPES

Another issue of long-standing interest has been the functions of stripes on zebras and tigers [29] (see also [15, 27, 55]). After digitizing the images of a tiger and zebra from Godfrey et al. [29], we analyzed four subsamples of the animals' dorsolateral sides and six samples of the background vegetation near their bodies. Results in Figure 6 indicate that the tiger and the zebra are not as cryptic against their backgrounds as *typica* morphs are against lichen-covered tree bark; instead, the zebra's and tiger's results are more comparable to those for *carbonaria* against polluted tree bark. With all frequency levels included in the analysis, the average C of the tiger is greater than that for the zebra. Note, however, that the background subsamples for the tiger are considerably less variable among themselves than is the case for the zebra image when all frequencies are included; thus, although the tiger is absolutely less different on average from the background than is the zebra when all frequencies are included, there is more opportunity for improvement in the tiger's match than for the zebra. As frequency information is removed, absolute crypticity (average C) for the tiger becomes less than that for the zebra, but the zebra's background subsamples are less variable among themselves than is the case for the tiger, and the zebra has greater apparent scope for improvement in crypsis. Crypsis at lower resolution may be especially important for both species—for tigers because their prey have small eyes or are nocturnally adapted, and for zebras because their most dangerous predators are most active at night (e.g., [67]).

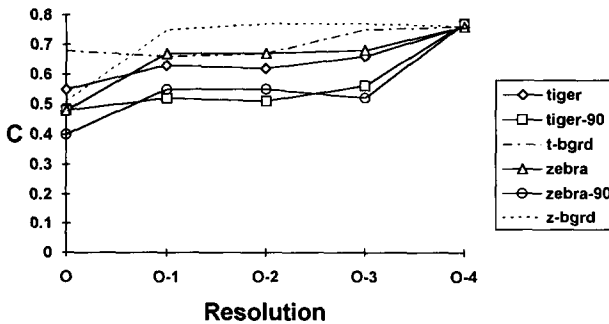


FIG. 6. Average crypsis index $C = 1 - D$ for four subsamples of images of tiger and zebra in Godfrey et al. [29] versus six subsamples of the backgrounds for each. "Tiger" and "zebra" refer to unrotated subsamples of each, and "tiger-90" and "zebra-90" refer to subsamples rotated by 90° . "T-bgrd" and "z-bgrd" represent averaged comparisons among background subsamples of the tiger and zebra images, respectively.

We also investigated the effect of orientation on crypticity of the tiger and zebra by 90° rotation of the animal's subsamples while leaving the background samples unchanged. Unlike the case for the peppered moth, orientation substantially affects crypsis for both the tiger and zebra (Figure 6). It seems probable that body orientation of animals like zebras and tigers will be less variable in comparison to their backgrounds than is the case for bark-resting moths.

LIMITATIONS AND SUGGESTIONS FOR FURTHER WORK

We end by emphasizing that a metric like the one we have proposed is most helpful specifically in testing hypotheses about visual textures per se. Such metrics do not necessarily indicate the absolute detectability of a particular object or organism because detectability can also be influenced by specific surface features, occluding edges, three-dimensional shape, color, movement, etc. The more general problem that the visual system must solve is that of figure-ground separation, or image segmentation. Image segmentation techniques based on biological-vision models are currently also an active area of research (e.g., [9, 19, 35, 47, 51, 54, 62, 65, 75]) although approaches that thoroughly integrate all of the above factors are still a long way off. If such methods are to be used to test hypotheses about crypsis or advertisement, they will also have to be adapted to produce a metric indicating the degree to which the organisms can be segmented from their visual backgrounds. One possibility for such a metric would be the portion of the true outline of an organism that is identified by the segmentation algorithm.

We thank J. Endler for helpful comments and G. Kiltie for assistance in preparing the manuscript.

REFERENCES

1. M. A. Arbib and A. R. Hanson, Vision in perspective in *Vision, Brain, and Cooperative Computation*, M. A. Arbib and A. R. Hanson, eds., MIT Press, Cambridge, Massachusetts, 1987, pp. 1–83.
2. J. Beck, A. Sutter, and R. Ivry, Spatial frequency channels and perceptual grouping in texture segregation, *Computer Vision, Graphics, and Image Processing* 37:299–325 (1987).
3. D. S. Blough, Discrimination of letters and random dot patterns by pigeons and humans, *J. Exp. Psychol.* 11:261–280 (1985).
4. D. S. Blough and J. J. Franklin, Pigeon discrimination of letters and other forms in texture displays, *Percept. Psychophys.* 38:523–532 (1985).
5. R. N. Bracewell, *The Fourier transform and Its Applications*, 2nd ed., McGraw-Hill, New York, 1986.
6. P. M. Brakefield, Industrial melanism: Do we have the answers? *Trends Ecol. Evol.* 2:117–122 (1987).

7. P. Brodatz, *Textures—A Photographic Album for Artists and Designers*, Dover, New York, 1966.
8. E. H. Burt, Jr., The adaptiveness of animal colors, *BioSci.* 31:723–729 (1981).
9. S. Casadei, S. Mitter, and P. Perona, Boundary detection in piecewise homogeneous textured images, in *Computer Vision-ECCV '92*, G. Sandini, ed., Springer-Verlag, New York, 1992, pp. 135–150.
10. R. R. Coifman and Y. Meyer, Orthonormal wave packet bases, preprint, Yale Univ., 1989.
11. R. R. Coifman and M. V. Wickerhauser, Best-adapted wavelet packet bases, preprint, Yale Univ., 1990.
12. R. R. Coifman and M. V. Wickerhauser, Entropy-based algorithms for best basis selection, *IEEE Trans. Inf. Theory* 38:713–718 (1992).
13. T. S. Collett, Orientation detectors in insects, *Nature* 362:494 (1993).
14. L. M. Cook, G. S. Mani, and M. E. Varley, Postindustrial melanism in the peppered moth, *Science* 231:611–613 (1986).
15. H. B. Cott, *Adaptive Coloration in Animals*, Oxford Univ. Press, New York, 1940.
16. C. Darwin, *The Origin of Species*, John Murray, London, 1859.
17. I. Daubechies, Orthonormal bases of compactly supported wavelets, *Comm. Pure Appl. Math.* 41:909–996 (1988).
18. R. L. DeValois and K. K. DeValois, *Spatial Vision*, Oxford Univ. Press, Oxford, England, 1988.
19. J. M. H. DuBuf, M. Kardan, and M. Spann, Texture feature performance for image segmentation, *Pattern Recognition* 23:291–309 (1990).
20. J. A. Endler, *Natural Selection in the Wild*, Princeton Univ. Press, Princeton, New Jersey, 1986.
21. J. A. Endler, On the measurement and classification of colour in studies of animal colour patterns, *Biol. J. Linn. Soc.* 41:315–352 (1990).
22. J. A. Endler, A predator's view of animal color patterns, *Evol. Biol.* 11:319–364 (1978).
23. J. A. Endler, Progressive background matching in moths, and a quantitative measure of crypsis, *Biol. J. Linn. Soc.* 22:187–231 (1984).
24. J. A. Endler, Signals, signal conditions, and the direction of evolution, *Amer. Natur.* 139:S125–S153 (1992).
25. J. A. Endler, Variation in the appearance of guppy color patterns to guppies and their predators under different visual conditions, *Vision Res.* 31:587–608 (1991).
26. R. Fox, Binocular vision and stereopsis, in *Frontiers of Visual Science*, S. J. Cool, E. L. Smith III, and D. L. MacAdam, eds., Springer-Verlag, New York, 1978, pp. 316–327.
27. G. Gibson, Do tsetse flies 'see' zebras? A field study of the visual response of tsetse to striped targets, *Physiol. Entomol.* 17:141–147 (1992).
28. J. J. Gibson, *The Perception of the Visual World*, Houghton Mifflin, Boston, 1951.
29. D. Godfrey, J. N. Lythgoe, and D. A. Rumball, Zebra stripes and tiger stripes: The spatial frequency distribution of the pattern compared to that of the background is significant in display and crypsis, *Biol. J. Linn. Soc.* 32:427–433 (1987).

30. R. Gurnsey and R. A. Browse, Micropattern properties and presentation conditions influencing visual texture discrimination, *Percept. Psychophys.* 41:239–252 (1987).
31. J. P. Hailman, *Optical Signals: Animal Communication and Light*, Indiana Univ. Press, Bloomington, Indiana, 1977.
32. P. J. Howlett and M. E. N. Majerus, The understanding of industrial melanism in the peppered moth (*Biston betularia*) (Lepidoptera: Geometridae), *Biol. J. Linn. Soc.* 30:31–44 (1987).
33. D. H. Hubel and T. N. Wiesel, Functional architecture of the macaque visual cortex, *Proc. Roy. Soc. London B* 198:1–59 (1977).
34. D. H. Hubel and T. N. Wiesel, Receptive fields, binocular interaction, and functional architecture in the cat's visual cortex, *J. Physiol. London* 160:106–154 (1962).
35. A. K. Jain and F. Farrokhnia, Unsupervised texture segmentation using Gabor filters, *Pattern Recognition* 24:1167–1186 (1991).
36. B. Julesz, *Foundations of Cyclopean Perception*, Univ. Chicago Press, Chicago, 1971.
37. B. Julesz, Textons, the elements of texture perception, and their interactions, *Nature* 290:91–97 (1981).
38. B. Kettlewell, *The Evolution of Melanism*, Clarendon Press, Oxford, England, 1973.
39. R. A. Kiltie, Camouflage comparisons among Mississippi delta fox squirrel morphs, *J. Mammal.* 73:906–913 (1992).
40. R. A. Kiltie, Countershading: Universally deceptive or deceptively universal? *Trends Ecol. Evol.* 3:21–23 (1988).
41. R. A. Kiltie, Testing Thayer's countershading hypothesis: An image processing approach, *Anim. Behav.* 38:542–544 (1989).
42. R. A. Kiltie, Tests of hypotheses on predation as a factor maintaining polymorphic melanism in coastal-plain fox squirrels, *Biol. J. Linn. Soc.* 45:17–37 (1992).
43. R. A. Kiltie and A. F. Laine, Visual textures, machine vision and animal camouflage, *Trends Ecol. Evol.* 7:163–166 (1992).
44. R. B. King, Lake Erie water snakes revisited: Morph- and age-specific variation in relative crypsis, *Evol. Ecol.* 6:115–124 (1992).
45. B. J. A. Krose, Local structure analyzers as determinants of preattentive pattern discrimination, *Biol. Cybern.* 55:289–298 (1987).
46. A. Laine and J. Fan, Texture classification by wavelet packet signatures, *IEEE Trans. Pattern Anal. Mach. Intell.* 15:1186–1191 (1993).
47. M. S. Landy and J. R. Bergen, Texture segregation and orientation gradient, *Vision Res.* 31:679–691 (1991).
48. J. Malik and P. Perona, Preattentive texture discrimination with early vision mechanisms, *J. Opt. Soc. Amer. A* 7:923–932 (1990).
49. S. G. Mallat, A theory for multiresolution signal decomposition: the wavelet representation, *IEEE Trans. Pattern Anal. Mach. Intell.* 11:674–693 (1989).
50. G. S. Mani and M. E. N. Majerus, Peppered moth revisited: Analysis of recent decreases in melanic frequency and predictions for the future, *Biol. J. Linn. Soc.* 48:157–165 (1993).
51. B. S. Manjunath and R. Chellappa, Unsupervised texture segmentation using Markov random field models, *IEEE Trans. Pattern Anal. Mach. Intell.* 13:478–482 (1991).

52. J. E. W. Mayhew and J. P. Frisby, Texture discrimination and Fourier analysis in human vision, *Nature* 275:438–439 (1978).
53. Y. Meyer, Principe d'incertitude, bases hilbertiennes et algebres d'operateurs, Paper presented at the Bourbaki seminar, 1985–1986, cited in [17].
54. R. Mohan, and R. Nevatia, Perceptual organization for scene segmentation and description, *IEEE Pattern Anal. Mach. Intell.* 13:616–635 (1992).
55. J. C. Mottram, Some observations on pattern-blending with reference to obliterative shading and concealment of outline, *Proc. Zool. Soc. London* 1915 (49):679–699 (1915).
56. K. Nakayama, S. Shimojo, and G. H. Silverman, Stereoscopic depth: Its relation to image segmentation, grouping, and the recognition of occluded objects, *Perception* 18:55–68 (1989).
57. D. Orsario and M. V. Srinivasan, Camouflage by edge enhancement in animal coloration patterns and its implications for visual mechanisms, *Proc. Roy. Soc. London B* 244:81–85 (1991).
58. V. S. Ramachandran, The neurobiology of perception, *Perception* 14:97–103 (1985).
59. V. S. Ramachandran, Perception: A biological perspective, in *Neural Networks for Vision and Image Processing*, MIT Press, Cambridge, MA, 1992, pp. 46–91.
60. V. S. Ramachandran, Visual perception in people and machines, in *AI and the Eye*, A. Blake and T. Troscianko, eds., Wiley, NY, 1990, pp. 21–77.
61. V. S. Ramachandran, Visual perception of surfaces: A biological theory, in *The Perception of Illusory Contours*, S. Petry and G. E. Meyer, eds., Springer-Verlag, New York, 1987, pp. 93–108.
62. T. R. Reed and H. Wechsler, Segmentation of textured images and gestalt organization using spatial/spatial-frequency representations, *IEEE Trans. Pattern Anal. Mach. Intell.* 12:1–12 (1990).
63. H. L. Resnikoff, *The Illusion of Reality*, Springer-Verlag, NY, 1989.
64. O. Rioul and M. Vetterli, Wavelets and signal processing, *IEEE Signal Processing Magazine* 8:14–38 (1991).
65. B. S. Rubenstein and D. Sagi, Spatial variability as a limiting factor in texture discrimination tasks: Implications for performance asymmetries, *J. Optical Soc. Amer. A* 7:1632–1643 (1990).
66. W. M. Saidel, How to be unseen: An essay in obscurity, in *Sensory Biology of Aquatic Animals*, J. Atema, R. R. Fay, A. N. Popper, and W. N. Tavolga, eds., Springer-Verlag, NY, 1987, pp. 487–513.
67. G. B. Schaller, *The Serengeti Lion*, Univ. Chicago Press, Chicago, 1972.
68. M. C. Srinivasan, Even insects experience visual illusions, *Curr. Sci.* 64:649–655 (1993).
69. J. Stromberg, A modified Franklin system and high-order spline systems of R_n as unconditional bases for Hardy spaces, in *Conference on Harmonic Analysis in Honor of Antoni Zygmund*, Vol. 2, W. Beckner, ed., Wadsworth, Belmont, CA, 1983, pp. 475–494.
70. S. S. Sweet, Geographic variation, convergent crypsis, and mimicry in Gopher snakes (*Pituophis melanoleucus*) and western rattlesnakes (*Crotalus viridis*), *J. Herpetol.* 19:55–67 (1985).
71. G. H. Thayer, *Concealing-coloration in the Animal Kingdom*, Macmillan, New York, 1909.

72. J. B. Thomas, *An Introduction to Communication Theory and Systems*, Springer-Verlag, New York, 1988.
73. P. P. Vaidyanathan, *Multirate Systems and Filter Banks*, Prentice Hall, Englewood Cliffs, New Jersey, 1993.
74. D. C. Van Essen, C. H. Anderson, and D. J. Felleman, Information processing in the primate visual system: An integrated systems perspective, *Science* 255:419-423 (1992).
75. H. Voorhees and T. Poggio, Computing texture boundaries from images, *Nature* 333:364-367 (1988).
76. H. Wechsler, Multiscale and distributed visual representations and mappings for invariant low-level perception, *Neural Networks for Perception*. Vol. 1. *Human and Machine Perception*, H. Wechsler, ed., Academic Press, New York, 1992, pp. 462-476.
77. F. Wilkinson, Visual texture segmentation in cats, *Behav. Brain Res.* 19:71-82 (1986).